Spherically expanding flame in silane–hydrogen–nitrous oxide–argon mixtures

Rémy Mével, Karl Chatelain, Simon Lapointe, Deanna A. Lacoste, Mahmoud Idir, Gabrielle Dupré, Nabiha Chaumeix

Spherically Expanding Flame in Silane–Hydrogen–Nitrous Oxide–Argon Mixtures

Article *in* Combustion and Flame · August 2020

DOI: 10.1016/j.combustflame.2020.07.032

7 authors, including:

R. Mével
Tsinghua University
134 PUBLICATIONS **703** CITATIONS
SEE PROFILE

Karl Chatelain
King Abdullah University of Science and Technology
29 PUBLICATIONS **95** CITATIONS
SEE PROFILE

Simon Lapointe
Lawrence Livermore National Laboratory
30 PUBLICATIONS **252** CITATIONS
SEE PROFILE

Deanna Lacoste
King Abdullah University of Science and Technology
126 PUBLICATIONS **2,289** CITATIONS
SEE PROFILE

Spherically Expanding Flame in Silane-Hydrogen-Nitrous Oxide-Argon Mixtures

R. Mével*,[a], K.P. Chatelain[b], S. Lapointe[c], D.A. Lacoste[b], M. Idir[d], G. Dupré[e], N. Chaumeix[d]

[a] *Center for Combustion Energy, School of Vehicle and Mobility, State Key Laboratory for Automotive Safety and Energy, Tsinghua University, Beijing, China*
[b] *King Abdullah University of Science and Technology (KAUST), Clean Combustion Research Center (CCRC), Thuwal, Saudi Arabia*
[c] *Lawrence Livermore National Laboratory, Livermore, USA*
[d] *Institut de Combustion, Aérothermique, Réactivité et Environnement, CNRS-ICARE, Orléans, France*
[e] *Université d'Orléans, Orléans, France*

Abstract

The effect of silane addition on the laminar flame speed (S_u^0) of flames propagating in hydrogen-nitrous oxide-argon mixtures has been investigated experimentally for the first time using the spherically expanding flame technique in a constant volume combustion chamber. Replacing hydrogen by silane and maintaining the equivalence ratio constant, much higher flame speeds, explosion peak pressures, and pressure rise coefficients were measured. A previously developed detailed reaction model has been updated based on ab initio thermodynamic properties calculations and collision limit violation analysis. The improved reaction model demonstrates encouraging performance in predicting the flame speed, with a mean absolute error below 11%. To explain the effect of silane addition on the flame dynamics, a number of parameters have been calculated including OH and H rate of production, heat release rate per reaction, and sensitivity coefficient on S_u^0. The dynamics of freely propagating flames in SiH_4-H_2-N_2O-Ar mixtures is essentially controlled by reactions of the H-O-N chemical system: $N_2O+H=N_2+OH$, $OH+H_2=H_2O+H$, and $N_2O(+M)=N_2+O(+M)$. Whereas silane addition does not influence much the rate of production of OH, it significantly modifies that of H with a number of pyrolytic chemical pathways of silicon hydrides, such as $SiH+H_2=SiH_2+H$ and $Si+H_2=SiH+H$,

*Corresponding author: mevel@mail.tsinghua.edu.cn

which act as sink of H atom as they proceed in the backward direction. The reactions forming SiO(s) and SiO_2(s), such as SiO+OH=SiO_2(s)+H and 2SiO=2SiO(s), are exothermic and significantly contribute to the temperature increase. The adiabatic, constant pressure flame temperature for mixture containing silane is significantly higher, up to several 100's K. The increase of S_u^0 induced by silane addition seems to be mostly related to the large increase of the flame temperature which leads to higher energy release rate.

Key words: Silane, Hydrogen, Flame speed, Expanding flame

---

1. Introduction

Accidental combustion events involving silane-oxydant mixtures, such as silane-air/oxygen or silane-nitrous oxide, have been reported for example by Hirano [1]. Although the pyrophoric behavior of silane (SiH_4) makes its handling very hazardous [2], it is commonly used as a source of silicon atom to form solid protective layers of SiO_2 onto semi-conductor components [3, 4]. Silane is also a potential additive for high-speed propulsion applications [5–7].

Although the combustion properties of silane-air/oxygen mixtures are not directly within the scope of the present paper, we note that they have been investigated in a number of previous studies: (i) the study of spontaneous ignition [2, 3, 8]; (ii) the measurement of the laminar flame speed and flammability limits [9]; and (iii) the measurement of ignition delay-time in shock tube for diluted SiH_4-O_2 [10] and SiH_4-Hydrocarbon Fuel-O_2 [5–7, 11] blends.

Concerning mixtures containing silane and nitrous oxide, many studies have been focused on high-temperature chemical kinetics under high-dilution conditions. Mick and Roth [12] employed direct absorption spectroscopy to measure Si and N concentrations and extract the rate constant for the reactions between Si and N_2O. Experiments were performed in the ranges T=1780-3560 K and P=50-171 kPa, respectively. Javoy et al. [13] and Mevel et al. [14] obtained oxygen atom profiles in shock-heated SiH_4-N_2O-Ar and SiH_4-H_2-N_2O-Ar over the temperature range 1606 and 2584 K and for pressures between 231 and 601 kPa. In addition, Horiguchi et al. [15] have measured the flammability limits of SiH_4-N_2O mixtures and reported that, at ambient temperature and pressure, the mixtures could be spark-ignited for silane content in the range 1.9-87.1%. More recently, Thomas et al. [16] studied the deflagration to detonation transition in silane-nitrous oxide mixtures with equivalence ratio Φ=1.11, and with various amounts of nitrogen dilution in the range X_{N2}=0-0.925. For initial pressure and temperature of 101 kPa and 283 K, respectively, they observed detonation-like pressure traces for X_{N2} up to 0.62. To the best of our knowledge, no data on the laminar flame speed nor on the explosion characteristics

of silane-nitrous oxide based mixtures are available in the literature.

The goals of the present study were (i) to measure the laminar flame speed of silane-hydrogen-nitrous oxide mixtures using the spherically expanding flame technique; (ii) to determine the explosion parameters of these mixtures; and (iii) to gain further insight into the silane oxidation mechanism under freely propagating flame conditions through numerical calculations. The manuscript is organized as follows: we first describe the experimental and modeling approaches that we employed; then we then present our results and discuss them in view of several thermo-chemical analyses; we finally conclude and propose some perspective for future work.

2. Materials and methods

2.1. Experimental approach

A schematic of the experimental set-up is shown in Fig. 1. The combustion vessel is a spherical stainless steel vessel of 250 mm inner diameter. Two windows made of quartz with a diameter of 70 mm and thickness of 30 mm, are mounted opposite to each other for visualizing the flame. During silane combustion, hot silica particles were formed and impacted onto the windows. For protection, smaller glass windows were added to the inside of the main windows, at the expense of the observation time. Prior to experiment, the vessel was evacuated to below 2 Pa. The visualization was achieved using a Z-type schlieren arrangement. The flame propagation was recorded by a Kodak or a Photron high speed camera with a framing rate of up to 13,500 fps or 24,000 fps, respectively. The beam of a pulsed Nd-YAG laser was focused onto the tip of a molybdenum electrode as the ignition source. The laser energy was maintained as low as possible to minimize the effect of input energy on the flame propagation. The flame expanded spherically from the hot spot resulting from the laser light-metal interaction. We have chosen to employ this unusual ignition system because we encountered difficulties to ignite the mixtures containing silane with our electric spark system. We attributed this issue either to the electrical resistance of silane or to the deposition of the electrically insulating condensed products onto the electrodes. It is noted that the ignition is triggered through the mechanism of hot

surface ignition [17] and is thus different from classical laser ignition [18]. The area of the heated surface, which leads to ignition, varies from one experiment to the other because of small alignment changes between the laser beam and the electrode. This leads in some cases to slightly elliptic flames. The pressure in the vessel was monitored using a Kistler piezo-electric pressure transducer with an uncertainty of ±3%. The pressure increase during the laminar flame speed measurement period was less than 2% of the initial pressure. The evolution of the flame radius (R_f) as a function of time was obtained using an in-house Matlab program described in [19], and was employed to extract the unstretched flame speed with respect to the burned gas (S_b^0). In order to determine which extrapolation equations are the best suited for the present experimental conditions, we calculated the Lewis number of the deficient reactant(s) using Cantera [20]. Since some of the mixtures contained two fuels, we adopted the so-called volume-based approach which was found to perform best for hydrogen-hydrocarbon mixtures by Bouvet et al. [21]. Further details can be found in the supplemental material. For all the SiH_4-H_2-N_2O-Ar mixtures, the Lewis number ranged between 0.5 and 2.5, which is consistent with the range of Lewis number examined theoretically by Chen [22]. For lean H_2-N_2O-Ar mixtures, the range of Lewis number is outside the one studied by Chen. However, the study of Varea et al. [23] has shown that for lean hydrogen-air mixtures, i.e. for low Lewis number, the Non-linear Quasi-steady equation (NQ) may be used although it leads to an uncertainty on the order of 10%. As a consequence, we followed the recommendations of Chen and used the Linear Curvature (LC) equation in the case of mixtures with high Lewis number (or positive Markstein length (L_B)), and the NQ equation in the case of mixtures with low Lewis number (or negative L_B). The LC and NQ equations are respectively given by

$$S_b = S_b^0 - 2\left(S_b^0 L_B\right)/R_f, \tag{1}$$

and

$$\ln\left(S_b\right) = \ln\left(S_b^0\right) - 2\left(S_b^0 L_B\right)/\left(R_f S_b\right), \tag{2}$$

where S_b is the stretched flame speed with respect to the burned gas. The unstretched laminar flame speed with respect to the unburned gas (S_u^0) was obtained

by dividing S_b^0 by the expansion ratio $\sigma = \rho_u/\rho_b$, where ρ_u and ρ_b are the density of the unburned gas and of the burned gas at thermodynamic equilibrium. Flame radii in the range $R_{f,min}$=10-15 to $R_{f,max}$=25-30 mm were typically used to extract the unstretched flame speed. Because silane-based mixtures are more difficult to handle than hydrocarbon ones, the uncertainty on S_u^0 is higher than typically observed. This is because (i) it is difficult to precisely control the silane content since a pipeline dead-volume could not be eliminated in the experimental arrangement (see next paragraph); (ii) the additional glass windows used to protect the quartz from hot particle impact reduce the image quality; (iii) the uncertainty on σ is larger for silane-based mixtures; and (iv) the radiative losses are more important for mixtures containing silane due to the formation of condensed combustion products. Table 1 lists the sources of uncertainty as well as their maximum and minimum values for mixtures with and without silane. A detailed explanation of the uncertainty calculation is available in the supplemental material. The uncertainty is ±11% at the stoichiometry, while it reaches ±15% for lean and rich mixtures. For the H_2-N_2O-Ar mixtures, under most conditions, the uncertainty is ±5%. This is consistent with the value we previously reported for these mixtures [19]. For the very lean mixtures, the uncertainty reaches ±12% due to radiative losses which were neglected in [19]. To be conservative, we have considered that this uncertainty represents only 1 σ_n, where σ_n^2 is the variance of a normal distribution, for silane-based mixtures. For H_2-N_2O-Ar mixtures, we have considered that this uncertainty represents 2 σ_n.

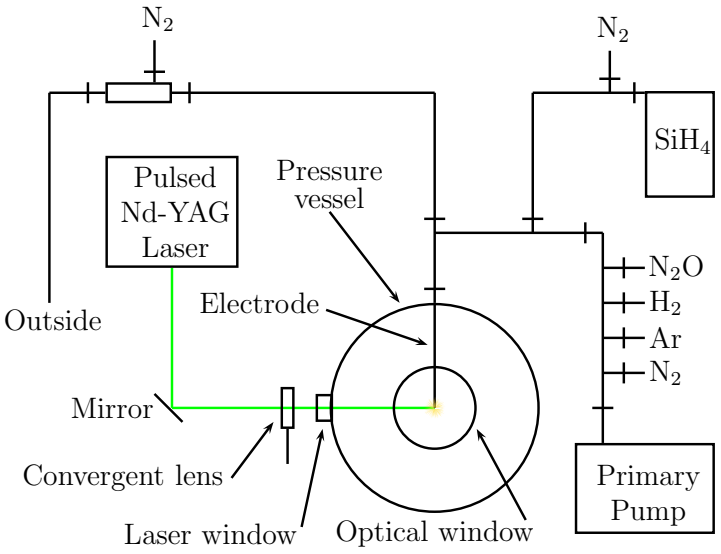

Figure 1: Schematic of the experimental set-up.

Source	H_2-N_2O-Ar mixtures	SiH_4-H_2-N_2O-Ar mixtures	Reference
P_1, T_1	0.4	0.4	[24]
Φ	1-2	1.5-4.5	Present study
Confinement	2	2	[25]
Ignition	0	0	[25]
Buoyuancy	0	0	[25]
Instability	0	0	[25]
Radiation	2-6	10	Adapted from [26] using [27]
NL stretch	1-2	1-2	Adapted from [25]
Extrapol eq	2-10	2-10	[25]
Radius detection	2	2	Adapted from [24]
Sigma	0	2	Present study
Total	5-12	11-15	

Table 1: Sources of uncertainty for the experimental determination of S_u^0. Uncertainty values are given in %. See supplemental material for details. NL stands for non-linear.

The mixtures were prepared from research-grade pure gases using the partial pressure method. The dilution by Ar was fixed at 60%, and Φ was varied between 0.3 and 2.4. The initial temperature was in the range 296-305 K and the pressure was 51 kPa, for safety reason. In the case of H_2-N_2O mixtures, Φ is simply defined as X_{H2}/X_{N2O}. For mixtures containing silane, the two following chemical reactions are considered to define the stoichiometric combustion:

$$H_2 + N_2O = H_2O + N_2 \tag{3}$$

$$SiH_4 + 4N_2O = SiO_{2(s)} + 2H_2O + 4N_2 \tag{4}$$

The equivalence ratio was defined for a given silane to hydrogen mole fraction ratio, R_{SH}, as:

$$\Phi = \frac{X_{H2}}{X_{N2O}} \times (1 + 4 \cdot R_{SH}) \tag{5}$$

Because of the pyrophoric nature of silane, it was not possible to pump down the filling line after introducing silane. As shown in Fig. 1, a special system of introduction and evacuation was designed. Silane was introduced by successive small amounts ($\leq$ 2.5 kPa). When the desired final pressure was reached, the silane remaining in the line was pushed with nitrogen into a parallel line until it reached a secondary vessel filled with N_2. The mixture was further diluted by a second N_2 stream and evacuated to the atmosphere through a 1 mm in diameter hole. After each experiments, the vessel was opened and thoroughly cleaned to remove the solid particles formed during combustion.

2.2. Modeling approach

The detailed reaction model corresponded to an update of the model of Mevel et al. [13, 14]. It includes 417 reactions and 89 species. The reactions from Mevel et al. [28] were used for the H-O-N system. For the silicon-containing species, the reactions came from Babushok et al. [29], Kondo et al. [30], Miller et al. [31], and Petersen et al. [32]. The reactions between the NO_x and the Si-compounds were taken from Mick et al. [12, 33] and Becerra et al. [34]. The reaction pathways given by Suh et al. [35] for the formation of silicon-containing condensed combustion products, SiO(s) and SiO_2(s), were employed. The thermodynamic data for most of the

species were updated using ab initio calculations performed with the G4 method. The rates of some reactions were found to violate the collision limit and were thus corrected. The transport properties were from: (i) Konnov [36] for the H-N-O system; (ii) Donovan et al. [37] for the Si-compounds; and (iii) from FlameMaster [38] for the species for which no data were available. The method employed to update the reaction model has been described in detail in [39].

Adiabatic, constant pressure, constant enthalpy (CP) as well as constant volume, constant internal energy (CV) equilibrium calculations were performed using Cantera [20]. These calculations are purely based on thermodynamic properties and may consider either one phase, gaseous, or two phases, gaseous and condensed. Three approaches were employed: (i) all species were gaseous and $SiO_{1,2}$(s) were the final products; (ii) all species were gaseous and $SiO_{1,2}$(g) were the final products; and (iii) all species were gaseous except $SiO_{1,2}$(s) which were treated as condensed, i.e. solid or liquid. The difference between (i) and (ii) is that different thermodynamic properties were used for the final products $SiO_{1,2}$(s) and $SiO_{1,2}$(g), whereas the difference between (i) and (iii) is the phase used to describe $SiO_{1,2}$(s).

A sparse, iterative flame solver [40] was employed to compute the laminar flame speeds. These calculations take into account the kinetics, thermodynamic, and transport properties of the species in the system. A mixture-averaged diffusion model was used and Soret effects were included. For all flame speed calculations, grid-independent solutions were ensured by using grids with more than 1000 points. For these calculations, all species were treated as gaseous. The difference between the flame speed results obtained when considering $SiO_{1,2}$(g) or $SiO_{1,2}$(s) is only due to the difference in the thermodynamic properties of the final products and is not a difference of phase, i.e. gaseous versus condensed. Other software like Chemkin or Cantera do not provide either a flame speed code for multi-phase media.

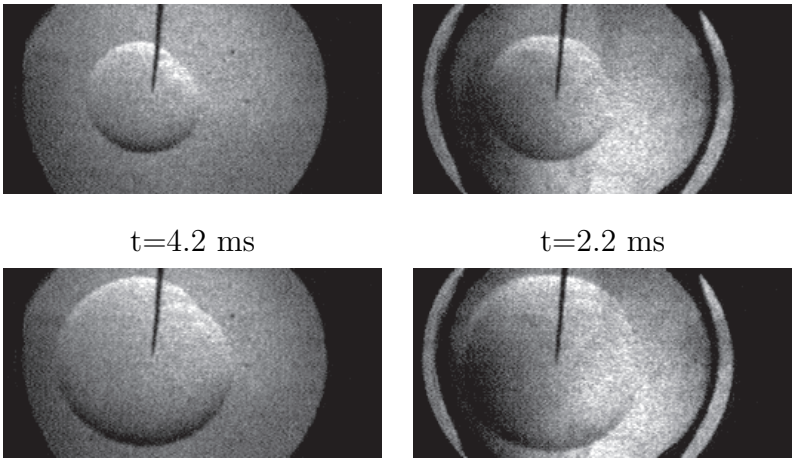

(a): H_2-N_2O-Ar (b): SiH_4-H_2-N_2O-Ar

Figure 2: Schlieren images of flames propagating in stoichiometric H_2-N_2O-Ar (a) and SiH_4-H_2-N_2O-Ar (b) mixtures. (a): X_{Ar}=0.6; T_1=302 K; P_1=51 kPa. (b): R_{SH}= 1/3; X_{Ar}=0.6; T_1=305 K; P_1=51 kPa.

3. Results and discussion

3.1. Experimental results and model predictions

Typical examples of flame propagation are shown in Fig. 2. Using Eq. 1 and 2, the unstretched flame speed has been extracted from the R_f=f(t) curves. Typical evolutions of S_b/S_b^0 as a function of stretch rate are shown in Fig. 3.

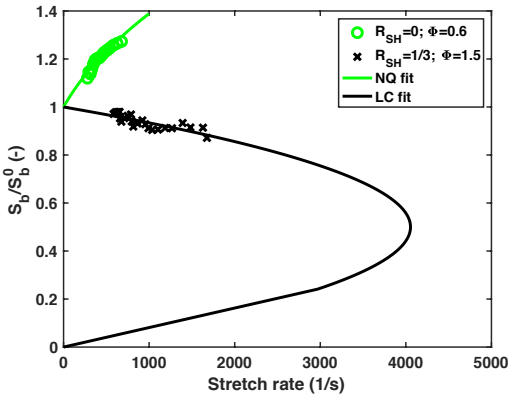

Figure 3: S_b/S_b^0 as a function of stretch rate for H_2-N_2O-Ar and SiH_4-H_2-N_2O-Ar. X_{Ar}=0.6; T_1=300 K; P_1=51 kPa.

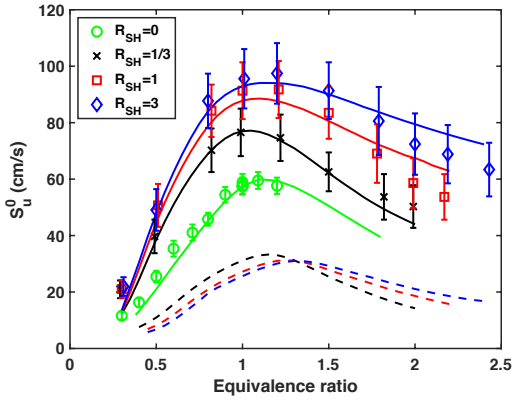

Figure 4: Experimental (symbols) and calculated (lines) S_u^0 for H_2-N_2O-Ar mixtures with and without SiH_4. X_{Ar}=0.6; T_1=300 K; P_1=51 kPa. Solid and dashed lines: calculations with $SiO_{1,2}$(s) and $SiO_{1,2}$(g) as final products.

Figure 4 summarizes the results obtained for the different silane to hydrogen ratios investigated, R_{SH}=0, 1/3, 1 and 3. It is noted that we have not attempted to cover the full range of flammability of the mixtures. The addition of silane in hydrogen-nitrous oxide mixtures induces a significant increase of S_u^0. For example, at Φ=1, replacing 25% of hydrogen by silane, R_{SH}=1/3, results in an increase of 32% of S_u^0. Above R_{SH}=1, S_u^0 remains essentially independent of the silane content, within the experimental uncertainty. The calculated laminar flame speeds are shown as solid lines in Fig. 4. Qualitatively, the detailed model captures the effect of SiH_4 addition on S_u^0. Quantitative assessment of the reaction model performance is summarized in Table 2 which gives, for each R_{SH}, (i) the mean difference

$$\bar{\Delta} = \frac{1}{N}\sum_{i=1}^{N} abs\left(S_u^0(Exp,i) - S_u^0(Cal,i)\right), \tag{6}$$

(ii) the mean relative error

$$\bar{E_r} = \frac{100}{N}\sum_{i=1}^{N} abs\left(\frac{S_u^0(Exp,i) - S_u^0(Cal,i)}{S_u^0(Exp,i)}\right), \tag{7}$$

and (iii) the mean error score [41]

$$\bar{E_S} = \frac{1}{N}\sum_{i=1}^{N}\left(\frac{S_u^0(Exp,i) - S_u^0(Cal,i)}{\sigma\left(S_u^0(Exp,i)\right)}\right), \tag{8}$$

where N is the number of data points; i is the number of experiment/calculation; *abs* indicates the absolute value; and σ is the uncertainty on the experimental measurement. Given that the chemistry of silicon-containing species is much less known

than the chemistry of hydrocarbons, the quantitative performances of the reaction model are encouraging since $\bar{\Delta}$, $\bar{E}_r$, and $\bar{E}_S$ are approximately 4.1 cm/s, 11%, and 1.8, respectively.

Series	$\bar{\Delta}$ (cm/s)	$\bar{E}_r$ (%)	$\bar{E}_s$
R_{SH}=0	2.8	12.3	3.4
R_{SH}=1/3	3.2	10.1	1.6
R_{SH}=1	5.6	11.9	1.3
R_{SH}=3	4.6	8.4	0.7
All	4.1	10.7	1.8

Table 2: Quantitative assessment of the reaction model performances in predicting S_u^0. $\bar{\Delta}$: mean difference; $\bar{E}_r$: mean relative error; $\bar{E}_s$: mean error score.

One of the important differences between the combustion of silicon compounds and that of hydrocarbons, is the nature of the combustion products. For silicon compounds, the most stable product is SiO_x(s), with $x \in$ [1,2] depending on the mixture equivalence ratio, which is condensed, whereas for hydrocarbons, the most stable product is gaseous CO_2. This indicates that part of the energy produced during the combustion of silane is due to the phase transition SiO_x(g)⇒SiO_x(s). To evaluate the importance of this process on the laminar flame propagation, we have performed calculations with a modified reaction model which does not include the condensation step. The oxidation process is thus terminated by the formation of SiO_x(g). The results of these calculations are shown as dashed lines in Fig. 4 and demonstrate the primary importance of the condensation process on the flame propagation. The flame speed calculated without condensed product formation is, on average, 2.8, 3.5, and 3.9 times lower for R_{SH}=1/3, 1, and 3, respectively, than when the formation of SiO_x(s) is included. This result is consistent with the observation of Babushok et al. [29] who pointed out the importance of the formation of the condensed silicon oxides in his study of the flame speed of silane-oxygen-nitrogen mixtures.

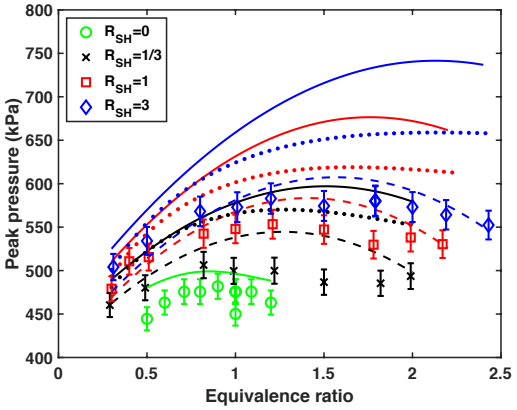

Figure 5: Experimental and calculated CV peak pressure for H_2-N_2O-Ar mixtures with and without SiH_4. X_{Ar}=0.6; T_1=300 K; P_1=51 kPa. Solid, and dotted lines are respectively the calculated P_{max} obtained when considering $SiO_{1,2}$(s) as gaseous and condensed species. The dashed line is the calculated P_{max} obtained when considering $SiO_{1,2}$(g) as the final products. It is noted that the experiments are subjected to various heat losses whereas the calculations were performed for an adiabatic system.

The importance of the formation of the condensed combustion products is also underlined in Fig. 5 which shows the experimental and calculated/theoretical peak pressures. Experimentally, the peak pressure values increase with the addition of silane. This increase is confirmed by the calculations, whatever the assumptions made on the thermodynamic properties or phase of the final products. Whereas the calculated results tend to indicate a shift of the maximum peak pressure toward higher equivalence ratio, it cannot be clearly confirmed experimentally due to the uncertainty on the pressure measurement. For mixtures without silane, the experimental peak pressures are within 5% of the theoretical values, whereas for mixtures containing silane, larger differences are seen when $SiO_{1,2}$(s) are considered as the final products. It is of 15% on average if $SiO_{1,2}$(s) are treated as gaseous species against 10% if $SiO_{1,2}$(s) are treated as condensed species. The highest difference is observed for the richest mixture at R_{SH}=3. On the other hand, when considering $SiO_{1,2}$(g) as the final products, the difference between the experimental and ideal values is below 4% on average. This seems to indicate that a significant fraction of the energy released by the silica particle formation is lost. This might be mostly attributed to the thermal radiation by the silicon oxide particles. Ngai et al. [27]

measured the radiative heat flux from silane-air and ethylene-air diffusion jet flames and found that it was 3.5 to 5 times higher for the silane flames. This is likely due to the high concentration of silicon-containing particles formed in the silane flames since, according to the CV calculations, most of the initial silane atoms are included in the silica particles at equilibrium.

We adopted the method described in [42] to extract the experimental pressure rise coefficient (K_g) which has an uncertainty of ±12% and is defined as

$$K_g = (dP/dt)_{max} V^{1/3}, \tag{9}$$

where V is the volume of the combustion vessel. Figure 6 shows the evolution of K_g with Φ for several silane contents. As silane content is increased, K_g increases. At Φ=1, respectively for R_{SH}=1/3, 1, and 3, K_g is 1.92, 2.75, 3.46 times higher than for the mixture without silane. For all R_{SH}, the K_g=f(Φ) curves demonstrate a typical inverse U-shape. The maximum K_g as a function of Φ seems to shift from Φ=0.9-1 for mixtures with R_{SH} <1 to Φ=1.2 for mixtures with R_{SH} ≥1. For comparison, a K_g of 75 MPa m/s was reported for a mixture of 3.7% silane in air [2].

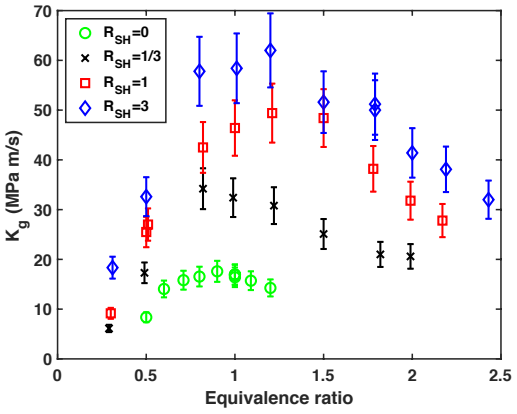

Figure 6: Pressure rise coefficient for H_2-N_2O-Ar mixtures with and without SiH_4. X_{Ar}=0.6; T_1=300 K; P_1=51 kPa.

3.2. Thermo-chemical analyses

To explain the effect of silane addition on the laminar flame dynamics, we performed a number of analyses including OH and H rate of production (OH and H

ROP), heat release rate per reaction (HRR), and sensitivity on S_u^0, for which the sensitivity coefficient for reaction i was defined as $C_S(i) = (k_i/S_u^0)(\partial S_u^0/\partial k_i)$ with k the rate constant. The distance-resolved ROP and HRR profiles are shown in Figure 7 to 9. In addition, the ROP and HRR were integrated over the domain used for the flame speed calculation. All quantities were normalized using the highest absolute value. The normalized ROP and HRR results are shown in Figure 10 in which the reactions were grouped within the following reaction classes: (i) reactions of the H-O-N system; (ii) reactions forming SiO_x(s); (iii) reactions describing the oxidation of Si-containing species; and (iv) reactions involving silicon hydrides. The reactions identified through the ROP, HRR, and sensitivity analyses are listed in Table 3.

R# in text	Reaction	Class
1	N_2O+H=N_2+OH	H-N-O system
2	OH+H_2=H_2O+H	H-N-O system
3	O+H_2=OH+H	H-N-O system
4	NH+NO=N_2O+H	H-N-O system
5	N_2O(+M)=N_2+O(+M)	H-N-O system
6	NH+OH=HNO+H	H-N-O system
7	SiO+OH=SiO_2(s)+H	Forming SiO_x(s)
8	2SIO=2SIO(s)	Forming SiO_x(s)
9	SiH_4+OH=SiH_3+H_2O	Oxidation of Si-containing species
10	SiH_3+O=H_2SiO+H	Oxidation of Si-containing species
11	SI+N_2O=SIO+N_2	Oxidation of Si-containing species
12	SiH+H_2=SiH_2+H	Involving silicon hydrides
13	Si+H_2=SiH+H	Involving silicon hydrides
14	SiH_4+M=SiH_2+H_2+M	Involving silicon hydrides

Table 3: List of important reactions identified through the ROP, HRR, and sensitivity analyses.

As seen in Fig. 7 and 10 a), for all R_{SH}, the production and consumption

of OH radical is dominated by the chemical reactions of the H-O-N system: R_1: $N_2O+H=N_2+OH$ and R_2: $OH+H_2=H_2O+H$. As R_{SH} is increased, R_3: $O+H_2=OH+H$ and R_4: $NH+NO=N_2O+H$, as well as two reactions involving Si-containing species, R_7: $SiO+OH=SiO_2(s)+H$ and R_9: $SiH_4+OH=SiH_3+H_2O$, become more important but their relative contributions to the overall OH dynamics remain weak, less than 22% as compared to R_1. Figure 8 and 10 b) show that, for all R_{SH}, the dynamics of H atom is dominated by R_1 and R_2. For $R_{SH} \geq 1$, two oxidative reactions involving Si-species, R_9 and R_{10}: $SiH_3+O=H_2SiO+H$, produce H atom but their combined contributions amount 25-30% that of R_1. More significant is the role of the pyrolytic pathways, R_{12}: $SiH+H_2=SiH_2+H$ and R_{13}: $Si+H_2=SiH+H$, which consume H atom with a combined contribution of up to 67% for R_{SH}=3.

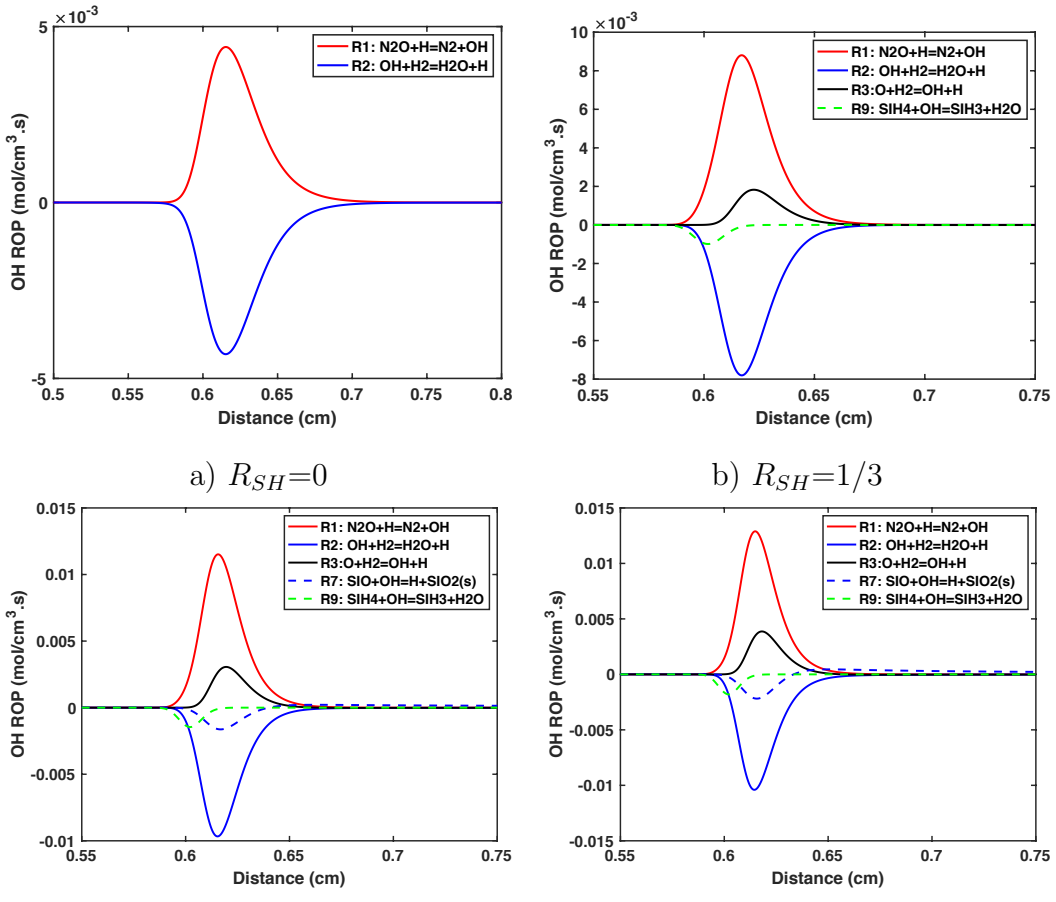

a) R_{SH}=0 b) R_{SH}=1/3

c) R_{SH}=1 d) R_{SH}=3

Figure 7: Distance-resolved OH ROP profiles for flames propagating in H_2-N_2O-Ar and SiH_4-H_2-N_2O-Ar mixtures. Φ=1; X_{Ar}=0.6; T_1=300 K; P_1=51 kPa.

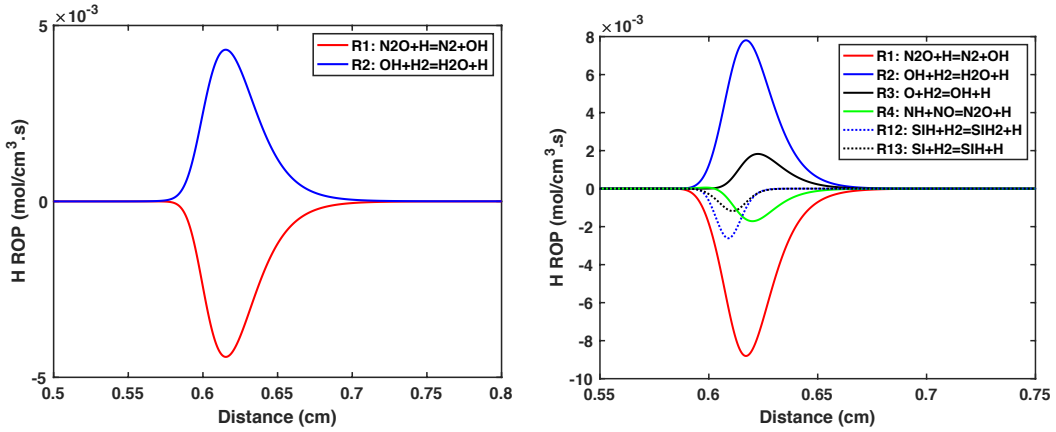

a) R_{SH}=0 b) R_{SH}=1/3

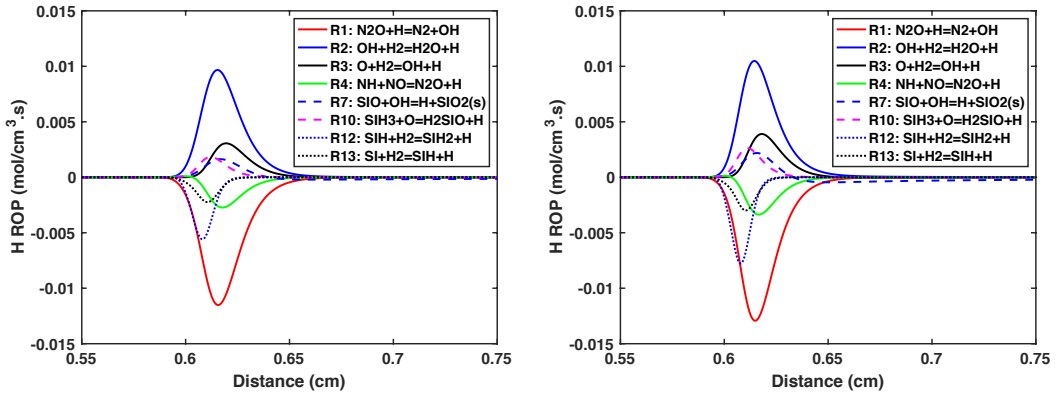

c) R_{SH}=1 d) R_{SH}=3

Figure 8: Distance-resolved H ROP profiles for flames propagating in H_2-N_2O-Ar and SiH_4-H_2-N_2O-Ar mixtures. Φ=1; X_{Ar}=0.6; T_1=300 K; P_1=51 kPa.

Figure 9 and 10 c) show the effect of silane addition on the HRR. For R_{SH}=0, the HRR is dominated by the linear chain R_1 and R_2. The contributions of these two reactions to the HRR are not much modified by the addition of silane. As silane content is increased, the contributions of R_5: $N_2O(+M)=N_2+O(+M)$, R_7, R_8: $2SiO=2SiO(s)$, R_{10}, R_{11}: $Si+N_2O=SiO+N_2$, R_{12}, and R_{14}: $SiH_4+M=SiH_2+H_2+M$ increase. The reactant decomposition reactions, R_5 and R_{14}, are the two main endothermic pathways. The reactions forming the condensed product $SiO_{1,2}(s)$, R_7 and R_8, constitute an important source of HRR, with a combined contribution in the range 36-71% of the HRR induced by R_1, respectively for R_{SH}=1/3 and 3. The combined contribution of the oxidative, R_{10} and R_{11}, and pyrolytic, R_{12}, chemical pathways to the overall HRR increases from 19 to 74% of HRR of R_1 as R_{SH} is increased from 1/3 to 3.

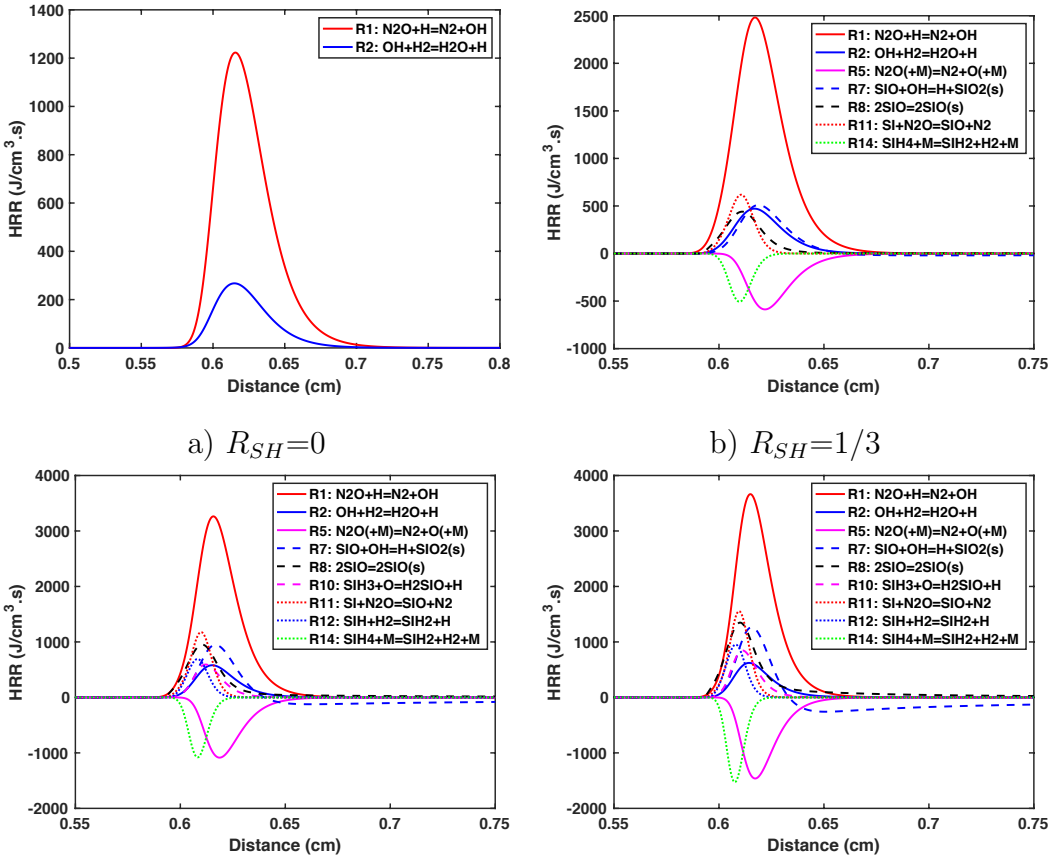

a) R_{SH}=0 b) R_{SH}=1/3

c) R_{SH}=1 d) R_{SH}=3

Figure 9: Distance-resolved HRR profiles for flames propagating in H_2-N_2O-Ar and SiH_4-H_2-N_2O-Ar mixtures. Φ=1; X_{Ar}=0.6; T_1=300 K; P_1=51 kPa.

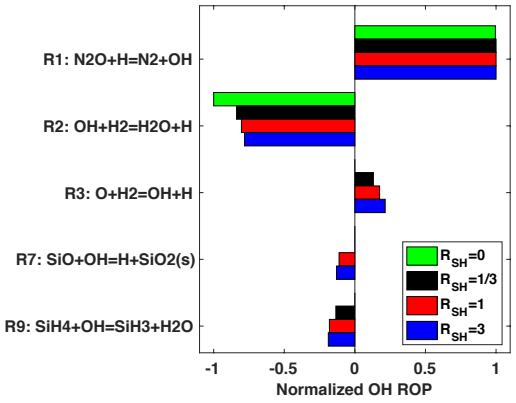

a) OH ROP

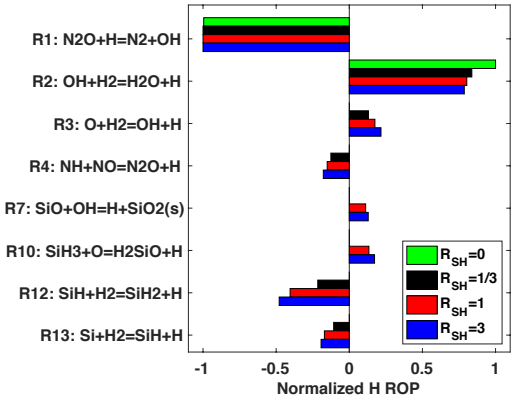

b) H ROP

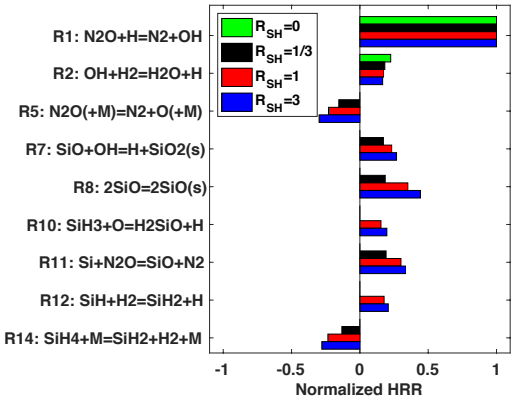

c) HRR

Figure 10: Normalized OH ROP, H ROP, and HRR for flames propagating in H_2-N_2O-Ar and SiH_4-H_2-N_2O-Ar mixtures. Φ=1; X_{Ar}=0.6; T_1=300 K; P_1=51 kPa.

Figure 11 shows the effect of silane addition on the normalized sensitivity coefficients on S_u^0. For all R_{SH}, the two most sensitive reactions are R_1 and R_5 which both belong to the H-O-N chemical system. Among the six other sensitive reactions, five of them involve the H atom. The reactions R_2 and R_7 both contribute to the increase of temperature and regenerate H atoms which further react with N_2O through R_1. The reactions R_4, R_{12}, and R_6: NH+OH=HNO+H, all act as a sink of H atom (in the backward direction), and thus exhibit a negative C_S. The reaction R_8 competes with R_7 for SiO consumption and prevents the regeneration of H atom. Thus, it demonstrates a negative C_S, despite its exothermicity.

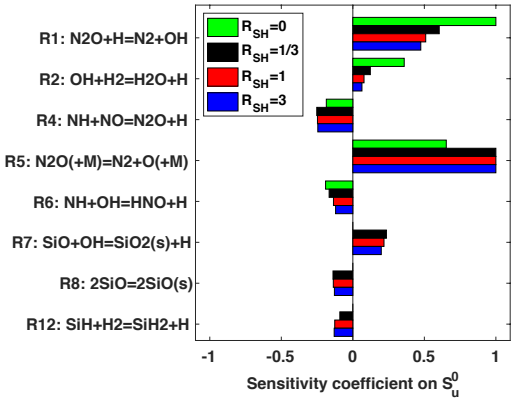

Figure 11: Normalized sensitivity coefficients on S_u^0 for flames propagating in H_2-N_2O-Ar and SiH_4-H_2-N_2O-Ar mixtures. Φ=1; X_{Ar}=0.6; T_1=300 K; P_1=51 kPa.

From the analyses shown in Fig. 7 to 11, it can be observed that the most important reactions for the dynamics of freely propagating flames in SiH_4-H_2-N_4O-Ar mixtures belong to the H-O-N chemical system, R_1, R_2, and R_5 for instance. While the ROPs of OH radical are not much affected by silane addition, endothermic pyrolytic chemical pathways of silicon hydrides constitute a significant sink of H atom. The reactions forming $SiO_{1,2}$(s) are exothermic and significantly contribute to the temperature increase. Figure 12 shows the adiabatic, CP flame temperature (T_f) calculated for the mixtures presently studied. T_f is significantly higher, up to several 100's K, for mixtures containing silane. Considering $SiO_{1,2}$(s) as gas or condensed products has little impact on T_f with a maximum difference of 0.5%. Considering $SiO_{1,2}$(g) as the final products, T_f is close to the case without silane. The increase

of S_u^0 induced by silane addition seems to be mostly related to the large increase of T_f which leads to higher energy release rate, overcoming the decrease of the thermal diffusivity induced by silane addition. While the predictions of the reaction model were overall encouraging, significant discrepancies were found for lean and rich mixtures at high silane contents. For the rich mixtures, these differences may be attributed to (i) radiative losses by the particle which were neglected; (ii) missing pathways for silicon hydrides which importance is highest in rich mixtures at high R_{SH}; (iii) the flame model which does not account for the phase change of $SiO_{1,2}$(s).

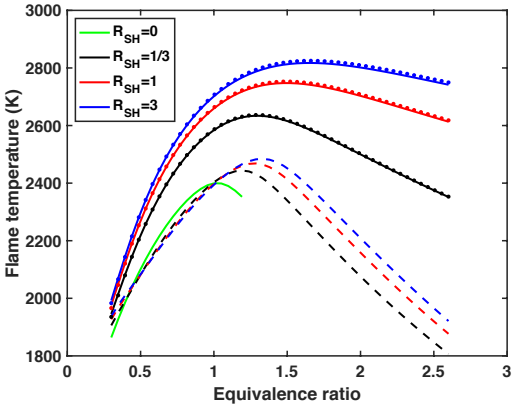

Figure 12: Adiabatic, CP flame temperature for H_2-N_2O-Ar and SiH_4-H_2-N_2O-Ar mixtures. X_{Ar}=0.6; T_1=300 K; P_1=51 kPa. Solid and dotted lines: T_f obtained when considering $SiO_{1,2}$(s) as gaseous and condensed species. Dashed line: T_f obtained when considering $SiO_{1,2}$(g) as the final products.

4. Conclusion

The laminar flame speed of hydrogen-nitrous oxide-argon mixture with and without silane has been investigated experimentally and numerically for the first time. At a fixed equivalence ratio, silane addition induces a large increase of the flame speed. Chemical kinetics analyses have shown that the flame dynamics is mostly controlled by the reactions of the H-O-N system. However, the much higher flame temperature induced by silane addition greatly enhances the energy release rate which leads to higher flame speed. The exothermic formation of condensed combustion products, $SiO_{1,2}$(s), appears as an important process for the flame propagation in silane-based

mixtures. Although the energy released during this process has been accounted for in our simulations by considering the thermodynamic properties of the condensed species, the actual phase change has been neglected due to a lack of available flame speed code. Future work should focus on developing such a code and evaluate the effect of the phase change on the flame speed. In addition, the losses associated with the emission by these condensed products should also be considered in future simulations.

Acknowledgments

Remy Mevel was supported by a start-up fund of the Center for Combustion Energy of Tsinghua University, the 1000 Young Talents Program of China, and the 1000 Young Talents Matching Fund of Tsinghua University. The work at Lawrence Livermore National Laboratory was supported by the U.S. Department of Energy and performed under contract DE-AC52-07NA27344. Partial support was provided by the King Abdullah University of Science and Technology, through the baseline fund BAS/1/1396-01-01. The authors are grateful to Pr Zheng Chen for useful discussions.

List of supplemental materials

- Table summarizing the experimental results
- Plot of Lewis number
- Plot of Markstein length
- Detailed error analysis for the flame speed measurements

References

[1] T. Hirano, Accidental explosions of semiconductor manufacturing gases in Japan, J. Loss Prevent. Proc. 17 (2004) 29–34.

[2] F. Tamanini, J. Chaffe, R. Jambar, Reactivity and ignition characteristics of silane/air mixtures, Process Saf. Prog. 17 (1998) 243–258.

[3] E. Ngai, K.P. Huang, J.R. Chen, C.C. Shen, H.Y. Tsai, S.K. Chen, S.C. Hu, P. Yeh, C.D. Liu, Y.Y. Chang, D. Peng, H.C. Wu, Field tests of release, ignition, and explosion from silane cylinder valve and gas cabinet, Process Saf. Prog. 26 (2007) 265–282.

[4] H. Tsai, Y. Lin, Y. Chang, J. Lin, J. Chen, E. Ngai, Unconfined silane-air explosions, J. Loss Prevent. Proc. 49 (2017) 700 – 710.

[5] E. Petersen, D. Kalitan, M. Rickard, Reflected-shock ignition of $SiH_4/H_2/O_2/Ar$ and $SiH_4/CH_4/O_2/Ar$ mixtures, J. Propuls. 20 (2004) 665–674.

[6] D. Kalitan, J. Hall, E. Petersen, Ignition and oxidation of ethylene-oxygen-diluent mixtures with and without silane, J. Propuls. 21 (2005) 1045–1056.

[7] M. Rickard, J. Hall, E. Petersen, Effect of silane addition on acetylene ignition behind reflected shock waves, Proc. Combust. Inst. 30 (2005) 1915–1923.

[8] J. Hartman, J. Famil-Ghiriha, M. Ring, H. O Neal, Stoichiometry and possible mechanism of SiH_4-O_2 explosions, Combust. Flame 68 (1987) 43–56.

[9] K. Tokuhashi, S. Horiguchi, Y. Urano, M. Iwasaka, H. Ohtani, S. Kondo, Premixed silane-oxygen-nitrogen flames, Combust. Flame 82 (1990) 40–50.

[10] E. Petersen, D. Kalitan, M. Rickard, M. Crofton, Silane oxidation behind reflected shock wave, Proceedings of the ISSW 24 (2004) 585–590.

[11] A. McLain, C. Jachimowski, R. Rogers, Ignition of SiH_4-H_2-O_2-N_2 behind reflected shock waves, Technical Report TP-2114, NASA, 1983.

[12] H. Mick, P. Roth, High-temperature kinetics of Si+N_2O, J. Phys. Chem. 98 (1994) 5310–5313.

[13] S. Javoy, R. Mével, G. Dupré, Oxygen atom kinetics in silane-hydrogen-nitrous oxide mixtures behind reflected shock waves, Chem. Phys. Lett. 500 (2010) 223–228.

[14] R. Mével, S. Javoy, G. Dupré, A chemical kinetic study of the oxidation of silane by nitrous oxide, nitric oxide and oxygen, Proc. Combust. Inst. 33 (2011) 485–492.

[15] S. Horiguchi, Y. Urano, K. Tokuhashi, S. Kondo, Explosion hazard of silane-nitrogen oxides gas mixture, Koatsu Gasu 26 (1989) 840–847.

[16] G. Thomas, R. Bambrey, G. Oakley, A study of flame acceleration and the possibility of detonation with silane mixtures, Process Saf. Environ. 117 (2018) 278–285.

[17] D. Roth, T. Harber, H. Bockhorn, Experimental and numerical study on the ignition of fuel/air mixtures at laser heated silicon nitride particles, Proc. Combust. Inst. 36 (2017) 1475–1484.

[18] N.D. Peters, B. Akih-Kumgeh, Characterization of spark- and laser-ignition of bio- and natural gas, Proceedings of ASME Turbo Expo 2017 117 (2017) GT2017-64902.

[19] R. Mével, F. Lafosse, N. Chaumeix, G. Dupré, C.E. Paillard, Spherical expanding flames in H_2-N_2O-Ar mixtures: Flame speed measurement and kinetic modeling, Int. J. Hydrog. Energy 34 (2009) 9007–9018.

[20] D.G. Goodwin, H.K.. Moffat, R.L. Speth, Cantera: An Object-oriented Software Toolkit for Chemical Kinetics, Thermodynamics, and Transport Processes, 2005.

[21] N. Bouvet, F. Halter, C. Chauveau, Y. Yoon, On the effective Lewis number formulations for lean hydrogen/hydrocarbon/air mixtures, Int. J. Hydrog. Energy 38 (2013) 5949–5960.

[22] Z. Chen, On the extraction of laminar flame speed and Markstein length from outwardly propagating spherical flames, Combust. Flame 158 (2011) 291–300.

[23] E. Varea, J. Beeckmann, H. Pitsch, Z. Chen, B. Renou, Determination of burning velocities from spherically expanding H_2/air flames, Proc. Combust. Inst. 35 (2015) 711–719.

[24] D. Nativel, M. Pelucchi, A. Frassoldati, A. Comandini, A. Cuoci, E. Ranzi, N. Chaumeix, T. Faravelli, Laminar flame speeds of pentanol isomers: An experimental and modeling study, Combust. Flame 166 (2016) 1–18.

[25] Z. Chen, On the accuracy of laminar flame speeds measured from outwardly propagating spherical flames: Methane/air at normal temperature and pressure, Combust. Flame 162 (2015) 2442–2453.

[26] H. Yu, W. Han, J. Santner, X.L. Gou, C.H. Sohn, Y. Ju, Z. Chen, Radiation-induced uncertainty in laminar flame speed measured from propagating spherical flames, Combust. Flame 161 (2014) 2815–2824.

[27] E. Ngai, R. Fuhrhop, J.R. Chen, J. Chao, C. Bauwens, C. Mjelde, G. Miller, J. Sameth, J. Borzio, M. Telgenhoff, B. Wilson, CGA G-13 large-scale silane release tests - Part I. Silane jet flame impingement tests and thermal radiation measurement, J. Loss Prevent. Proc. 36 (2015) 478–487.

[28] R. Mével, S. Javoy, F. Lafosse, N. Chaumeix, G. Dupré, C.E. Paillard, Hydrogen-nitrous oxide delay time: shock tube experimental study and kinetic modelling, Proc. Combust. Inst. 32 (2009) 359–366.

[29] V. Babushok, W. Tsang, D. Burgess, M. Zachariah, Numerical study of low- and high-temperature silane combustion, Proc. Combust. Inst. 27 (1998) 2431–2439.

[30] S. Kondo, K. Tokuhashi, A. Takahashi, M. Kaise, A numerical study of low temperature silane combustion, Combust. Sci. Technol. 159 (2000) 391–406.

[31] T. Miller, M. Wooldridge, J. Bozzelli, Computational modelling of the SiH_3+O_2 reaction and silane combustion, Combust. Flame 137 (2004) 73–92.

[32] E.L. Petersen, D.M. Kalitan, M.J.A. Rickard, M.W. Crofton, Silane oxidation behind reflected shock waves, in: Z. Jiang (Ed.), Shock waves, Springer, Berlin, 2005, pp. 585–590.

[33] H. Mick, H. Matsui, P. Roth, High-temperature kinetics of Si atom oxidation by NO based on Si, N, and O atom measurements, J. Phys. Chem. 97 (1993) 6839–6842.

[34] R. Becerra, H. Frey, B. Mason, R. Walsh, Absolute rate constant and temperature dependence for the reaction of silylene with nitrous oxide, Chem. Phys. Lett. 185 (1991) 415–420.

[35] S.M. Suh, M. Zachariah, S. Girshick, Modeling particle formation during low pressure silane oxidation: detailed chemical kinetics and aerosol dynamics, J. Vac. Sci. Technol. A 19 (2001) 940–951.

[36] A. Konnov, Detailed reaction mechanism for small hydrocarbons combustion. release 0.5., 2000.

[37] M. Donovan, D. Hall, P. Torek, C. Schrock, M. Wooldridge, Demonstration of temperature and OH mole fraction diagnostic in $SiH_4/H_2/O_2$/Ar flames using narrow-line UV OH absorption spectroscopy, Proc. Combust. Inst. 29 (2002) 2635–2643.

[38] H. Pitsch, URL: http://www. itv. rwth-aachen. de/en/downloads/flamemaster (1998).

[39] K.L. Chatelain, R. Mevel, D.A. Lacoste, Correction of reaction models using collision limit violation analyses: ap- plication to a silane reaction model, Combust. Flame 217 (2020) 346 – 359.

[40] S. Lapointe, R. Whitesides, M. McNenly, Sparse, iterative simulation methods for one-dimensional laminar flames, Combust. Flame 204 (2019) 23 – 32.

[41] C. Olm, I.G. Zsély, R. Pálvolgyi, T. Varga, T. Nagy, H.J. Curran, T. Turányi, Comparison of the performance of several recent hydrogen combustion mechanisms, Combust. Flame 161 (2014) 2219 – 2234.

[42] S.P.M. Bane, R. Mével, S.A. Coronel, J.E. Shepherd, Flame burning speeds of undiluted and nitrogen diluted hydrogen-nitrous oxide mixtures, Int. J. Hydrog. Energy 36 (2011) 10107–10116.